ChemComm

Accepted Manuscript

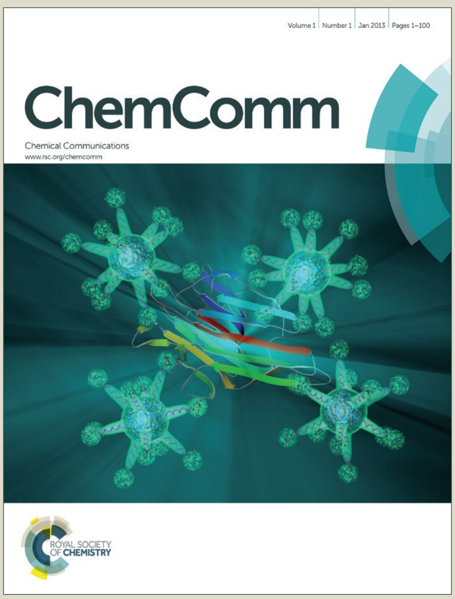

ChemComm

COMMUNICATION

Photochemical H_2 Evolution from Water Catalyzed by Dichloro(diphenylbipyridine)platinum(II) Derivative Tethered to Multiple Viologen Acceptors

Received 00th January 20xx,
Accepted 00th January 20xx

DOI: 10.1039/x0xx00000x

www.rsc.org/

Kyoji Kitamoto*[ab] and Ken Sakai*[abc]

A new single-component photocatalyst for water reduction to H_2, dichloro(dpbpy)platinum(II) derivative (dpbpy = 4,4'-diphenyl-2,2'-bipyridine) tethered to four pendant viologen acceptors (1), is shown to exhibit twice higher photocatalytic efficiency than the previously reported dichrolo(bpy)-platinum(II) analog (2; bpy = 2,2'-bipyridine), consistent with the higher absorptivity of 1 at the metal-to-ligand charge transfer (^{1}MLCT) band due to the larger π-conjugation in dpbpy relative to bpy.

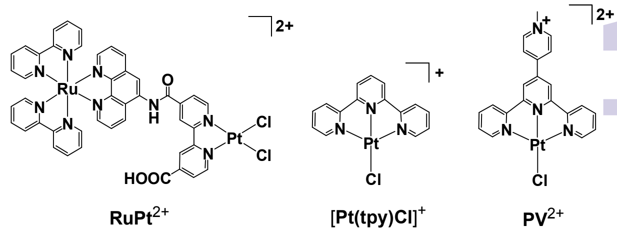

Fig. 1 Structures of Pt(II)-based PHEMDs.

In order to fabricate practical solar energy conversion processes, extensive efforts have been made to develop molecule-based systems that can split water into H_2 and O_2 under solar light illumination.[1−3] Since the late 1970s, multi-component systems made up of a photosensitizer, an electron relay, and an H_2-evolving catalyst, such as a colloidal Pt or a molecular catalyst, have been extensively investigated in order to advance studies focusing on the photo-driven H_2 evolution half-cell.[4,5] In this context, one of our recent interests has concentrated on fabricating single-component molecular photocatalysts driving photoreduction of water to H_2 in the presence of a sacrificial electron donor. We term such systems as "photo-hydrogen-evolving molecular devices" (abbreviated as PHEMDs), which must possess bifunctionality to serve as both a photosensitizer and an H_2-evolving catalyst. The first generation of PHEMDs developed by us are classified as "pigment-catalyst dyads", such as **RuPt**$^{2+}$ depicted in Fig. 1.[6]

The second generation series is composed of simple mononuclear platinum(II) complexes, such as [**PtCl(tpy)**]$^+$ (ref. 7a; tpy = 2,2';6',2"-terpyridine) and **PV**$^{2+}$ having the same [PtCl(tpy)]$^+$ unit (ref 8; see Fig. 1), for which major photo-driven steps are shown to take place within the ion-pair adducts formed between the positively charged PHEMD and the dianionic form of EDTA (i.e., YH_2^{2-}; 93% in abundance at pH 5.0); the electron transfer (ET) is considered to proceed via the reductive quenching of the so-called ^{3}MLCT or ^{3}MMLCT excited state of the [PtCl(tpy)]$^+$-based chromophore (MMLCT = metal-metal-to-ligand charge transfer specific to the stacked dimer species formed in solution[7a]). An intriguing finding in the study of **PV**$^{2+}$ is that it produces H_2 via forming a doubly-reduced species **PV**^{0}, which is given via two consecutive photo-driven electron transfer (PET) steps: [**PV**$^{2+}$…YH_2^{2-}] (ion-pair adduct) + hν → [**PV**$^{2+}$*…YH_2^{2-}] → **PV**$^{+}$• + YH_2^-, and [**PV**$^+$•…YH_2^{2-}] + hν → [**PV**$^+$•*…YH_2^{2-}] → **PV**^{0} + YH_2^- followed by H_2 evolution according to **PV**^{0} + 2H$^+$ → **PV**$^{2+}$ + H_2.[8b]

Next, we classify the third generation series as those having at least one electron-reservoir site, e.g., a viologen unit, within the above-mentioned Pt-only PHEMDs. The $PtCl_2$(bpy) (bpy = 2,2'-bipyridine) derivatives tethered to multi-viologen units, such as [**PtCl$_2$(bpyMV4)**]$^{8+}$ (**2**) depicted in Fig. 2, correspond to such series and were proven to exhibit improved photocatalytic performance.[9] The third generation series show to attain much higher turnover numbers (TONs) in photocatalysis of H_2 formation (TON = 14−2[illegible]) compared to the first and second generation series which exhibited TONs = 3−4.1. The catalytic enhancement achieved by attaching electron-reservoir sites to PHEMDs was rationally interpreted by the fact that the photosensitizing chromophore (i.e., $PtCl_2$(bpy) for **2**) can be regenerated from its reduced form (i.e., $PtCl_2$(bpy$^-$•)) immediately after the first PET step by use of simple intramolecular ET, as illustrated in Scheme 1. Thus, an identical chromophore can be utilized in the second PET step (see Scheme 1). Whereas, **PV**$^{2+}$ loses the initial chromophore in the second PET step, since a colored radical intermediate **PV**$^+$•, possessing broad visible and near infrared (NIR) absorption bands is afforded in the first PET. This was judged

[a] Department of Chemsitry, Faculty of Science, Kyushu University, Motooka 744, Nishi-ku, Fukuoka 819-0395, Japan. E-mail: kyo_kitamoto@chem.kyushu-univ.jp, ksakai@chem.kyushu-univ.jp
[b] International Institute for Carbon-Neutral Energy Research (WPI-I2CNER), Kyushu University, Motooka 744, Nishi-ku, Fukuoka 819-0395, Japan.
[c] Center for Molecular Systems (CMS), Kyushu University, Motooka 744, Nishi-ku, Fukuoka 819-0395, Japan.

† Electronic Supplementary Information (ESI) available. See DOI: 10.1039/x0xx00000x

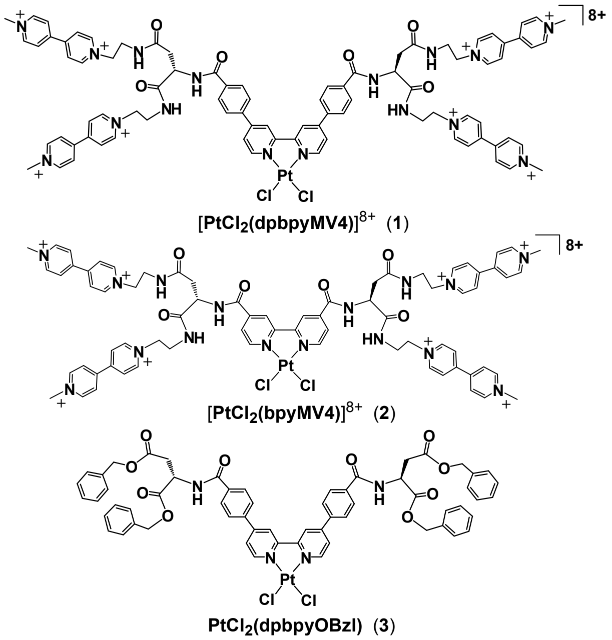

Fig. 2 Structures of pigment-acceptor-catalyst triads and a control complex having no viologen tethers investigated in this study.

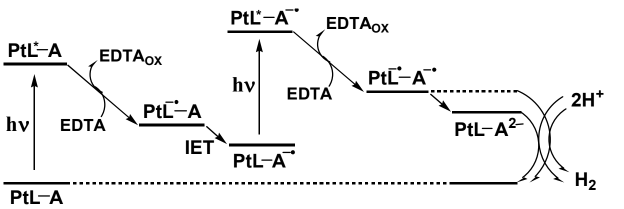

Scheme 1. Energy level diagrams for the photochemical H_2 production driven by pigment-acceptor-catalyst triads, where A is an acceptor and L (the ligand) corresponds to bpy, 2,2':6',2''-terpyridine (tpy), etc.

to be the major cause of lower quantum efficiency in the second PET, giving rise to the lower overall photocatalytic efficiency.[9]

In spite of our continued efforts, the TONs achieved in our systems are still relatively low, which is in part due to the low absorptivity at the ^{1}MLCT band of the $PtCl_2$(bpy) unit in **2** (λ_{max} = 386–388 nm, ε = 2300–3800 $M^{-1}cm^{-1}$).[9] Thus, we focus here on the effect of raising the absorptivity of the photosensitizing unit in this third generation series of PHEMDs. To improve the light-harvesting property, we have designed and synthesized a new pigment-acceptor-catalyst triad having a $PtCl_2$(dpbpy) chromophore, **[PtCl₂(dpbpyMV4)]**$^{8+}$ (**1**), depicted in Fig. 2. A larger π-conjugation in dpbpy is expected to afford a higher absorptivity at the ^{1}MLCT band of $PtCl_2$(dpbpy) relative to that of $PtCl_2$(bpy). We also discuss the effect of elongation in the donor-acceptor distance by insertion of phenylene moieties upon modifying **2** to give **1**.

Fig. 3 shows the absorption spectra of **1** and **2** in aqueous 0.1 M NaCl solution. At every wavelength around the ^{1}MLCT band (ca. 350–400 nm), the molar absorptivity of **1** is roughly twice as high as that of **2**. It is shown that **1** obeys Beer's law at whole wavelength domain at concentrations below 0.2 mM, precluding dimer formation of **1** in solution under these conditions (Fig. S6). An aqueous solution of either **1** or **2** does not exhibit emission at room temperature. Whereas, **1** in a methanol/ethanol/N,N-dimethylformamide (MED; 4:4:1) glass

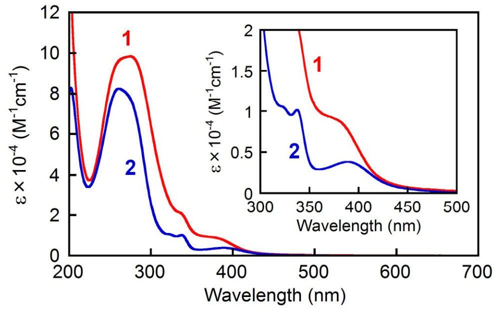

Fig. 3 Absorption spectra of **[PtCl₂(dpbpyMV4)]**$(PF_6)_8$ (**1**) and **[PtCl₂(bpyMV4)]**$(PF_6)_8$ (**2**; values taken from ref. 9a) in a 0.1 M aqueous NaCl solution at 20 ºC in air. The inset shows magnification in the 300–500 nm region.

at 77 K shows emission with the 0-0 and 0-1 vibronic emission peaks centered at 501 and 536 nm (Fig. S9). The emission decay profile shows a triple-exponential feature with the lifetimes estimated as τ_1 = 1.38 (4.7 %), τ_2 = 6.06 (31.8 %), and τ_3 = 12.8 μs (63.5 %), where values in parenthesis are relative contributions (Fig. S10 and Table S1). A large Stokes shift (ca. 100 nm) and a long-lived character reveal that the emission arises from the triplet excited (^{3}MLCT) state. A quite similar features with comparable lifetimes are also observed for a control complex having no viologen tethers, **PtCl₂(dpbpyOBzl)** (**3**) (τ_1 = 1.01 (2.4 %), τ_2 = 5.38 (28.4 %), and τ_3 = 12.3 μs (69.2 %); see Fig. S12 and Table S1). This preclude the occurrence of ET involving the viologen moieties under these conditions.

The cyclic voltammogram of **1** displays four reduction waves (Fig. S13). The first and second reductions, observed at −0.85 and −1.25 V vs. Fc/Fc^+, are assignable to the consecutive one-electron reductions at each viologen moiety, which correspond to the MV^{2+}/MV^{+}• and MV^{+}•/MV^0 couples, respectively. The reduction at dpbpy ligand is observed at −1.46 V vs. Fc/Fc^+, slightly shifted to the negative side compare to that of bpy in **2** (−1.35 V vs. Fc/Fc^+). The dpbpy/dpbpy$^-$• couple for the control complex **3** is also observed at −1.46 V vs. Fc/Fc^+ (see Fig. S14 and Table S2). Finally, the fourth reduction corresponds to the Pt^{II}/Pt^{I} couple, as previously reported for the related platinum(II) complexes.[9,11,12] Using the electrochemical parameters obtained for **2**, the free energy change given by IET (ΔG_{IET}) can be estimated as ΔG_{IET} = −F{$E_{1/2}$(MV^{2+}/MV^{+}•) − $E_{1/2}$(dpbpy/dpbpy$^-$•)} = −0.61 eV, where F is a Faraday constant. This confirms that the $PtCl_2$(dpbpy$^-$•) moiety has much higher driving force for H_2 evolution compared with a reducing equivalent stored in the form of MV^{+}•. In other words, H_2 evolution by $PtCl_2$(dpbpy$^-$•)–$(MV^{2+})_3(MV^{+}$•) is much more thermodynamically favourable when compared with that by $PtCl_2$(dpbpy)–$(MV^{2+})_2(MV^{+})_2$.

The photo-hydrogen-evolving (PHE) activity of **1** in the presence of EDTA at pH 5.0 was investigated under visible light irradiation (λ > 400 nm). As shown in Fig. 4a, **1** exhibits much higher PHE activity than **2**, where the TON of **1** (TON = 35, 12 h) is about twice as high as that of **2** (TON = 18, 12 h). The lack of colloidal platinum dispersion during the photocatalytic H_2 evolution was confirmed by DLS (dynamic light scattering) measurements. The variations in the light scattering intensity during the photolysis were judged to be negligible (Fig. S15), revealing that formation of colloidal platinum nanoparticles is negligible. These observations well support the homogeneous nature of **1** during photocatalytic H_2 evolution.

On the other hand, as the NaCl concentration is increased, the PHE activity increases and shows a maximum at an NaCl concentration ca. 20 mM (Fig. S16). As previously reported,[5d] it is quite likely that the hydrolysis equilibrium in eqn. (1) is shifted to the left side at higher Cl^- concentrations to raise the concentration of the dichlorido species, which are considered to exhibit higher PHE activity compare to the hydrolysis products in the right side of eqn. (1).

$$[PtCl_2(dpbpyMV4)]^{8+} + 2X \rightleftarrows [PtX_2(dpbpyMV4)]^{n+} + 2Cl^- \quad (1)$$
$$(X = Cl^-, H_2O, OH^-, CH_3COO^-, \text{etc.})$$

Upon further raising the NaCl concentration in the range 20−100 mM, the PHE activity decreases monotonically (Fig. S16). In this concentration range, gradual increase in the light scattering intensity due to dispersion of particles (ca. 55.0−5150 nm) was observed during the photolysis (Fig. S15). This is attributable to partial deposition of reduced species which have a lower positive charge relative to **1** and thus possess lower solubility in aqueous media. The validity of this argument was afforded by observing disappearance of particle dispersion by DLS after reoxidizing the reduced species by exposing the photolysis solution to air.

In order to confirm the reason for the enhanced photocatalytic performance of **1**, the action spectrum (the wavelength dependence of the quantum yield of H_2 evolution) was developed (Fig. 4b). The photolysis was carried out using various combinations of cut-off and band-pass filters to select the wavelength region, as summarized in Table S3 and Figs. S17−S21. The flux of photon absorbed by the photolysis solution under each irradiation condition was determined by the chemical actinometry using potassium tris(oxalato)ferrate(III).[13] The action spectrum can be well correlated with the absorption feature of **1** (Fig. 4b), confirming that the photochemical process driven by **1** proceeds through the formation of the ^{3}MLCT state of **1**.

Spectral changes observed during the photocatalysis (Fig. S22a) shows initial fast growth of visible and NIR bands, derived from the MV^{+}• and/or $(MV^+)_2$ components. These bands thereafter gradually decay over 60−80 min to about a half of the maximum absorbance attained after the initial 5-min irradiation. As previously observed for **2** and other $PtCl_2$(bpy) derivatives tethered to Asp-based multi-viologen units,[9a,12] preferential formation of π-dimer $(MV^+)_2$ can be recognized by the major absorptions at 360, 520, and 900 nm. Spectral deconvolution was carried out to determine the relative abundances of MV^{+}• and $(MV^+)_2$ components (Fig. S22b). Although, the–total number of electrons stored per molecule (NES) becomes plateau at 60−80 min, we realize that the MV^{+}• concentration (i.e., a singly reduced Asp−(MV^{2+})(MV^{+}•) branch) rises and saturates around 20 min, which can be correlated to the induction period of H_2 production (Fig. 4a). In other words, the $(MV^+)_2$ component has a minor contribution to the observed H_2 evolution. This is a reasonable consideration because the reduction potential of $(MV^+)_2$ π-dimer is 0.15 V positive-shifted compared to that of the free MV^{+}• species.[9b,14] Combined with our previous observations for this third generation series,[9] it seems most likely that the major H_2 evolution proceeds via forming $PtCl_2$(dpbpy$^-$•)−(MV^{+}•)(MV^{2+})$_3$ which react with two proton to afford both H_2 and the original form of **1**, which is further supported by the following spectroscopic studies.

Picosecond transient absorption (TA) studies provide insights into the initial rapid photoinduced processes. For acetonitrile solutions of **1** and **3** at room temperature, laser pulse excitation at 400 nm causes broad positive absorption in the range 450−800 nm (Figs. S25a,26a), attributable to the formation of the ^{3}MLCT state. For both cases, the decay at 62[illegible] nm obeys a quadruple-exponential feature. Moreover, the lifetimes together with the contributions observed for **1** well resemble to the corresponding values observed for **3**; τ_1 = 2.[illegible] (33.6 %), τ_2 = 45.9 (32.8 %), τ_3 = 114 (21.8 %), and τ_4 = 1070 ps (11.8 %) for **1** and τ_1 = 2.67 (52.9 %), τ_2 = 25.4 (18.6 %), τ_3 = 93.2 (18.9 %), and τ_4 = 1120 ps (9.6 %) for **3** (Figs. S25b,26b). Similarity in the decay features suggests that oxidative quenching of the ^{3}MLCT state (i.e., $PtCl_2$(dpbpy)[illegible]) by the viologen tethers in **1** does not proceed. On the other hand, TA data for the aqueous system could only be obtained for **1** since **3** is insoluble in water. Similarly, the triplet of **1** in water decays with a quadruple-exponential feature (see Fig. S27). Importantly, upon adding EDTA to this system, dramatically different behaviors are observed (Fig. S28), in which reductive quenching of ^{3}MLCT by EDTA proceeds to give the initial photoproduct $PtCl_2$(dpbpy)−(MV^{2+})$_3$(MV^{+}•) which does not decay within the 3-ns measurement window. Thus, the reductive quenching that proceeds within a few picosecond time domain is a major path leading to photocatalytic H_2 evolution.

Nanosecond TA spectroscopy was used to further examine the initial photoproduct. Upon pulsing at 355 nm, the 400- and 600-nm bands specific to MV^{+}•,[15] are observed only in the presence of EDTA (3−30 mM; see Fig. S29a). Moreover, the

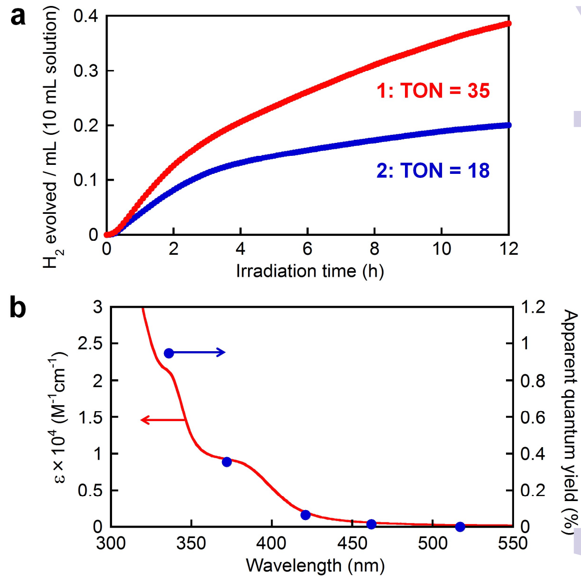

Fig. 4 (a) Visible light-driven H_2 production (> 400 nm) from an aqueous acetate buffer solution (0.03 M CH_3COOH and 0.07 M CH_3COONa; pH 5.0, 10 mL, at 20 ºC under Ar) containing 30 mM EDTA in the presence of 0.05 mM **[PtCl₂(dpbpyMV4)]**Cl_8 (**1**) or 0.05 mM **[PtCl₂(bpyMV4)]**$(PF_6)_8$ (**2**). (b) The action spectrum (wavelength dependence) of the quantum yield for H_2 production photocatalyzed by **1** is overlaid with its molar absorptivity spectrum, recorded for an aqueous 0.1 M NaCl solution of **1** at 20 ºC. The solution conditions are same to those given in Fig. 4a, where the optical properties of the interference glass filters used are supplied as Table S3 and Figs. S17−S21. The quantum yields were estimated from the initial rates of H_2 production using the photon flux summarized in Table S3.

yield of the photoproduct having an MV^{+}• site, estimated from the increase in absorbance at 400 nm, shows saturation at higher EDTA concentrations above 30 mM (Fig. S29b), consistent with the saturation kinetics observed for **2** and other Pt(II)-based PHEMDs.[6c,7,8b,9a] These observations allow us to conclude that **1** also forms an ion-pair adduct with YH_2^{2-} in order to promote reductive quenching within the adduct, leading to formation of a very short-lived unobservable photoproduct $PtCl_2(dpbpy^{-}•)-(MV^{2+})_4$ which probably rapidly undergoes rapid IET to yield the initial photoproduct $PtCl_2(dpbpy)-(MV^{2+})_3(MV^{+}•)$.

In the above single laser pulsing experiments, the major portion (91−92%) of the initial photoproduct decays due to the recombination expressed by a reaction: $EDTA^{+}• + PtCl_2(dpbpy)-(MV^{2+})_3(MV^{+}•) \rightarrow EDTA + PtCl_2(dpbpy)-(MV^{2+})_4$ (Fig. S30), as observed in the earlier study.[4b] This clearly indicates that the second electron injection to $\mathbf{1}^{-}$ from $EDTA^{+}•$ ($EDTA^{+}• + \mathbf{1}^{-} \rightarrow EDTA^{2+} + \mathbf{1}^{2-}$) is not thermally driven under these conditions. In other words, the ET from $EDTA^{+}•$ to $\mathbf{1}^{-}$ can only proceed as a light-induced process ($EDTA^{+}• + \mathbf{1}^{-} + h\nu \rightarrow EDTA^{+}• + \mathbf{1}^{-}* \rightarrow EDTA^{2+} + \mathbf{1}^{2-}$), where $\mathbf{1}^{-}$ denotes $PtCl_2(dpbpy)-(MV^{2+})_3(MV^{+}•)$, while $\mathbf{1}^{2-}$ denotes $PtCl_2(dpbpy^{-}•)-(MV^{2+})_3(MV^{+}•)$ or $PtCl_2(dpbpy)-(MV^{2+})_2(MV^{+})_2$. Recombination is only partly inhibited, presumably due to the partial loss of $EDTA^{+}•$ before the recombination event (see Fig. S30).

As pointed out above, the $dpbpy^{-}•$-driven reduction has a driving force 0.61 eV higher than the $MV^{+}•$-driven reduction so that a $(dpbpy^{-}•)(MV^{+}•)$-driven water reduction ($PtCl_2(dpbpy^{-}•)-(MV^{2+})_3(MV^{+}•) + 2H^{+} \rightarrow PtCl_2(dpbpy)-(MV^{2+})_4 + H_2$) is the most efficient path to H_2 evolution, as recently discussed for another PHEMD.[9b] The elongation in the net distance between $PtCl_2(bpy)$ donor and the viologen acceptors by the insertion of phenylene units is considered to lower the efficiency in the ET from the donor to the acceptor, which may also contribute to the improved photocatalytic activity of **1** compared to **2**.

An intriguing finding here is that one-electron-reduced $MV^{+}•$ species rather than the two-electron-reduced $(MV^{+})_2$ species plays a major role in the photocatalysis of H_2 production driven by **1**. We are now attempting to further raise the overall energy conversion efficiency of our PHEMDs by further raising the absorptivity of the photosensitizing chromophore and also by incorporating the more red-shifted chromophores in order to harvest a wider wavelength range of the solar spectrum.

This work was supported by a Grant-in-Aid for Scientific Research (B) (No. 24350029) and a Grant-in-Aid for Scientific Research on Innovative Areas 'Artificial Photosynthesis' (No. 2406, 24107004) from the Ministry of Education, Culture, Sports, Science, and Technology (MEXT) of Japan. This was also supported by the International Institute for Carbon Neutral Energy Research (WPI-I2CNER), sponsored by the World Premier International Research Center Initiative (WPI), MEXT, Japan. K.K. acknowledges Research Fellowships of the Japan Society for the Promotion of Science for Young Scientist. We thank Prof. Keiji Tanaka and Mr. Yudai Ogata (Department of Applied Chemistry, Kyushu University) for the kind assistance in the picosecond TA measurements.

Notes and references

1 J. J. Concepcion, R. L. House, J. M. Papanikolas and T. J. Meyer, *Proc. Natl. Acad. Sci. U.S.A.*, 2012, **109**, 15560.

2 (a) A. J. Esswein and D. G. Nocera, *Chem. Rev.*, 2007, **107**, 4022; (b) V. Artero, M. Chavarot-Kerlidou and M. Fontecave, *Angew. Chem. Int. Ed.*, 2011, **50**, 7238; (c) M. Wang, L. Chen and L. Sun, *Energy Environ. Sci.*, 2012, **5**, 6763; (d) J. R. McKone, S. C. Marinescu, B. S. Brunschwig, J. R. Winkler and H. B. Gray, *Chem. Sci.*, 2014, **5**, 865; (e) W. T. Eckenhoff and R. Eisenberg, *Dalton Trans.* 2012, **41**, 12793; (f) D. L. DuBois, *Inorg. Chem.*, 2014, **53**, 3935.

3 (a) K. J. Young, L. A. Martini, R. L. Milot, R. C. Snoeberger III, V. S. Batista, C. A. Schmuttenmaer, R. H. Crabtree and G. W. Brudvig, *Coord. Chem. Rev.*, 2013, **256**, 2503; (b) D. J. Wasylenko, R. D. Palmer and C. P. Berlinguette, *Chem. Commun.*, 2013, **49**, 218; (c) J. J. Concepcion; J. W. Jurss; M. K. Brennaman; P. G. Hoertz; A. O. T. Patrocinio; N. Y. Murakami Iha; J. L. Templeton and T. J. Meyer *Acc. Chem. Res.*, 2009, **42**, 1954; (d) A. Sartorel, M. Bonchio, S. Campagna and F. Scandola, *Chem. Soc. Rev.*, 2013, **42**, 2262; (e) H. Lv, Y. V. Geletii, C. Zhao, J. W. Vickers, G. Zhu, Z. Luo, J. Song, T. Lian, D. G. Musaev and C. L. Hill, *Chem. Soc. Rev.*, 2012, **41**, 7572.

4 (a) M. Kirch, J.-M. Lehn and J.-P. Sauvage, *Helv. Chim. Acta*, 1979, **62**, 1345; (b) K. Kalyanasundaram, J. Kiwi and M. Grätzel, *Helv. Chim. Acta*, 1978, **61**, 2720; (c) C. V. Krishnan, B. S. Brunschwig, C. Creutz and N. Sutin, *J. Am. Chem. Soc.*, 1985, **107**, 2005.

5 (a) K. Sakai and K. Matsumoto, *J. Coord. Chem.*, 1988, **18**, 169; (b) K. Sakai and K. Matsumoto, *J. Mol. Catal.*, 1990, **62**, 1; (c) K. Sakai, Y. Kizaki, T. Tsubomura and K. Matsumoto, *J. Mol. Catal.*, 1993, **79**, 141; (d) K. Sakai and H. Ozawa, *Coord. Chem. Rev.*, 2007, **251**, 2753.

6 (a) H. Ozawa, M. Haga and K. Sakai, *J. Am. Chem. Soc.*, 2006, **128**, 4926; (b) S. Masaoka, Y. Mukawa and K. Sakai, *Dalton Trans.*, 2010, **39**, 5868; (c) H. Ozawa, M. Kobayashi, B. Balan, S. Masaoka and K. Sakai, *Chem. Asian J.*, 2010, **5**, 1860; (d) H. Ozawa and K. Sakai, *Chem. Commun.*, 2011, **47**, 2227; (e) G. Ajayakumar, M. Kobayashi, S. Masaoka and K. Sakai, *Dalton Trans.*, 2011, **40**, 3955; (f) C. V. Suneesh, B. Balan, H. Ozawa, Y. Nakamura, T. Katayama, M. Muramatsu, Y. Nagasawa, H. Miyasaka and K. Sakai, *Phys. Chem. Chem. Phys.*, 2014, **16**, 1607.

7 (a) R. Okazaki, S. Masaoka and K. Sakai, *Dalton Trans.*, 2009, 6127; (b) K. Yamauchi and K. Sakai, *Dalton Trans.*, 2015, **44**, 8685.

8 (a) M. Kobayashi, S. Masaoka and K. Sakai, *Dalton Trans.*, 2012, **41**, 4903; (b) M. Kobayashi, S. Masaoka and K. Sakai, *Angew. Chem. Int. Ed.*, 2012, **51**, 7431.

9 (a) K. Kitamoto and K. Sakai, *Angew. Chem. Int. Ed.*, 2014, **53**, 4618; (b) K. Yamamoto, K. Kitamoto, K. Yamauchi and K. Sakai, *Chem. Commun.*, 2015, **51**, 14516.

10 D. R. McMillin and J. J. Moore, *Coord. Chem. Rev.*, 2002, **229**, 113.

11 (a) P. S. Braterman, J.-I. Song, F. M. Wimmer, S. Wimmer, W. Kaim, A. Klein and R. D. Peacock, *Inorg. Chem.* 1992, **31**, 5084; (b) P. S. Braterman, J.-I. Song, C. Vogler, W. Kaim, *Inorg. Chem.* 1992, **31**, 222; (c) L. Yang, F. L. Wimmer, S. Wimmer, J. Zhao and P. S. Braterman, *J. Organomet. Chem.* 1996, **525**, 1.

12 M. Ogawa, G. Ajayakumar, S. Masaoka, H.-B. Kraatz and K. Sakai, *Chem. Eur. J.*, 2011, **17**, 1148.

13 C. G. Hatchard and C. A. Parker, *Proc. R. Soc. London, Ser. A.*, 1956, **235**, 518.

14 W. S. Jeon, H.-J. Kim, C. Lee and K. Kim, *Chem. Commun.*, 2002, 1828.

15 (a) C. Lee, C. Kim, M. S. Moon and J. W. Park, *Bull. Korean. Chem. Soc.*, 1994, **15**, 909; (b) C. Lee, Y. M. Lee, M. S. Moon, S. H. Park, J. W. Park, K. G. Kim and S.-J. Jeon, *J. Electroanal. Chem.*, 1996, **416**, 139; (c) C. Lee, M. S. Moon and J. W. Park, *J. Electroanal. Chem.* 1996, **407**, 161; (d) J. W. Park, N. H. Choi and J. H. Kim, *J. Phys. Chem.*, 1996, **100**, 769.

Table of contents

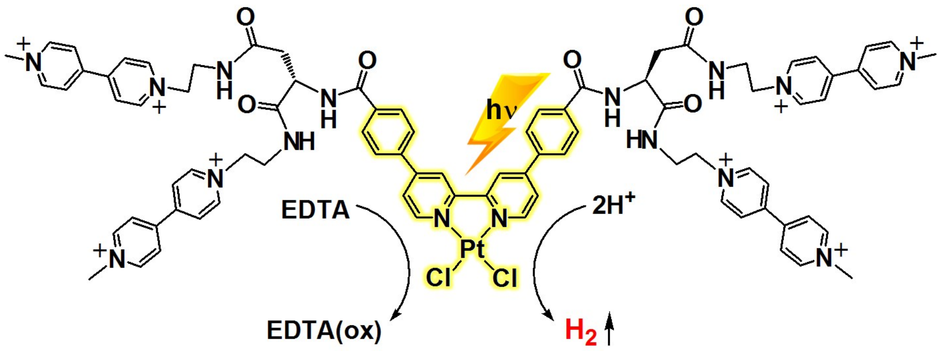

Photocatalytic Enhancement Based on Chromophore Engineering

Enhanced hydrogen evolution from water photocatalyzed by a dichloro(diphenylbipyridine)platinum(II) derivative tethered to multiple viologen acceptors is reported.